Photodissociation of HI and DI: Polarization of atomic photofragments

Alex Brown[a)]
Department of Chemistry, University of Alberta, Edmonton, Alberta T6G 2G2, Canada

(Received 14 September 2004; accepted 30 November 2004; published online 14 February 2005)

The complete angular momentum distributions and vector correlation coefficients (orientation and alignment) of ground state $I(^2P_{3/2})$ and excited state $I(^2P_{1/2})$ atoms resulting from the photodissociation of HI have been computed as a function of photolysis energy. The orientation and alignment parameters $\mathbf{a}_Q^{(K)}(p)$ that describe the coherent and incoherent contributions to the angular momentum distributions from the multiple electronic states accessed by parallel and perpendicular transitions are determined using a time-dependent wave packet treatment of the dissociation dynamics. The dynamics are based on potential energy curves and transition dipole moments that have been reported previously [R. J. LeRoy, G. T. Kraemer, and S. Manzhos, J. Chem. Phys. **117**, 9353 (2002)] and used to successfully model the scalar (total cross section and branching fraction) and lowest order vector (anisotropy parameter β) properties of the photodissociation. Predictions of the $\mathbf{a}_Q^{(K)}(p)$, parameters for the isotopically substituted species DI are reported and contrasted to the analogous HI results. The resulting polarization for the corresponding H/D partners are also determined and demonstrate that both H and D atoms produced can be highly spin polarized. Comparison of these predictions for HI and DI with experimental measurement will provide the most stringent test of the current model for the electronic structure and the interpretation of the dissociation based on noncoupled excited state dynamics. © *2005 American Institute of Physics*. [DOI: 10.1063/1.1850465]

I. INTRODUCTION

Hydrogen iodide represents one of the simplest systems that dissociates to yield open shell fragments and, thus it provides a model system for studying molecular photodissociation dynamics on multiple potential energy curves (PECs). Its photochemistry has been the subject of many experimental and theoretical studies.[1–22] In particular, the photodissociation process

$$\mathrm{HI} + h\nu \rightarrow \mathrm{H}(^2S) + \mathrm{I}(^2P_{3/2}) \rightarrow \mathrm{H}(^2S) + \mathrm{I}(^2P_{1/2})$$

is of interest. Following standard nomenclature, the two spin-orbit states of iodine, $I(^2P_{3/2})$ and $I(^2P_{1/2})$, are referred to as I and I^*, respectively. The goals of the experimental and theoretical studies were to understand the roles of the various electronic states involved in the excitation and the possible nonadiabatic transitions that could take place between the excited PECs as the molecule fragments. While the first experimental studies focused on measurement of the continuum absorption,[1–4] (the so-called *A*-band absorption) more recent experimental studies have examined the photodissociation process in more detail by measuring the relative yields of the two spin-orbit states that can be produced and the photofragment angular distributions.[5–15]

Despite the wealth of experimental measurements, little has changed in the qualitative interpretation of the photodissociation process since Mulliken's work in 1937.[16] His interpretation was that the *A*-band absorption was due to contributions from three overlapping continuum transitions into the $a\,^3\Pi_1$, $A\,^1\Pi_1$, and $a\,^3\Pi_{0^+}$ states (given in order of increasing energy). There was also the possibility of absorption into the $t\,^3\Sigma_1$ state but it was predicted to lie at too high an energy to contribute to absorption in the *A* band. These qualitative predictions have been confirmed by high-level *ab initio* calculations for HI.[18] While Mulliken predicted qualitatively the states contributing, a detailed interpretation of the dissociation process including a quantitative understanding of the contributions of these electronic states requires measurements beyond the total continuum absorption. The two fragmentation channels resulting from absorption in this energy region must be investigated. The production of ground state iodine $I(^2P_{3/2})$ arises from the perpendicular ($\Delta\Omega=1$) excitations $A\,^1\Pi_1 \leftarrow X\,^1\Sigma_{0^+}$ and $a\,^3\Pi_1 \leftarrow X\,^1\Sigma_{0^+}$. On the other hand, excited state iodine $I(^2P_{1/2})$ is produced primarily from a parallel ($\Delta\Omega=0$) excitation $a\,^3\Pi_{0^+} \leftarrow X\,^1\Sigma_{0^+}$ but could also be produced from a perpendicular ($\Delta\Omega=1$) excitation $t\,^3\Sigma_1 \leftarrow X\,^1\Sigma_{0^+}$. It is the relative roles these electronic states play in the photodissociation process, that experiment and theory have tried to determine.

As mentioned above, the focus of the experimental studies has been on the determination of scalar properties, i.e., the total cross section and the branching fraction Γ measuring the yield of spin-orbit excited atoms (I^*) relative to the total yield. There have also been several measurements[9–15] of the vector property β. For prompt dissociation of a diatomic molecule following absorption of linearly polarized light, the fragment recoil velocity angular distribution to lowest order is given by

[a)]Electronic mail: alex.brown@ualberta.ca

$$I(\theta) = (\sigma/4\pi)[1 + \beta P_2(\cos\theta)], \quad (1)$$

where θ is the angle between the laser's polarization direction and the recoil velocity vector, σ is the partial absorption cross section for formation of a given product, and β is the anisotropy parameter. The value of β can range between -1 and 2 where $\beta=-1$ corresponds to a pure perpendicular transition while $\beta=2$ corresponds to a pure parallel transition. While the measurement of the scalar properties and β provide a wealth of information on the molecular structure, i.e., PECs, transition dipole moments, and, if applicable, nonadiabatic couplings, underlying the dynamics, there has been an explosion of interest in measuring the alignment and/or orientation of halogen atoms resulting from the dissociation of diatomic molecules.[23–30]

Since the halogen atoms possess angular momenta, they can have a preferred orientation and/or alignment in space. It has been shown[31] that the spatial distribution of the photofragment angular momenta can be described by contributions from dissociation on a single potential energy surface (PES) and from the interference from dissociation via multiple PESs. The polarization of the halogen atom, or any other atom resulting from photodissociation that possesses angular momentum, can be fully described in the molecular frame by the $\mathbf{a}_Q^{(K)}(p)$ parameters[32] where K and Q refer to the spatial distributions in the molecular frame and p refers to the symmetry of the transition dipole moment from the ground electronic state to the dissociating state. The symmetry p can be $\parallel$, $\perp$, or ($\parallel$, $\perp$) corresponding to pure parallel, pure perpendicular, or mixed parallel/perpendicular excitation.

In the present work, the $\mathbf{a}_Q^{(K)}(p)$ parameters ($K\leqslant 3$) describing the alignment/orientation of iodine fragments, both I and I^*, produced from the photodissociation of HI and DI are reported. They are determined from a quantum mechanical time-dependent wave packet calculation based on recently published[17] empirical potential energy curves and transition dipole moments. These molecular parameters were determined by fitting the experimentally measured scalar properties, i.e., total cross-section and branching fractions, for the HI and DI photofragmentation processes. Calculations based on them were then shown to reproduce the lowest order anisotropy parameter β.

The paper is organized in the following manner. Section II A outlines the underlying electronic structure as it relates to the two lowest energy asymptotes $H(^2S_{1/2})+I(^2P_{3/2})$ and $H(^2S_{1/2})+I(^2P_{1/2})$, which are the only ones of interest here. The time-dependent wave packet treatment of the dissociation dynamics and the determination of the total cross section, the partial absorption cross sections, the I^* branching fraction, and the lowest order anisotropy parameter β from these calculations are discussed in Sec. II B. Section II C presents the methods used to determine the dynamical factors $f_K(q,q')$ from the photofragmentation **T** matrix elements, and the corresponding $\mathbf{a}_Q^{(K)}(p)$ parameters relevant to HI (DI) dissociation that can be determined. The results as a function of photolysis wavelength for the HI and DI molecules are presented and contrasted in Sec. III. In Sec. III A, the theoretical results for the total cross sections, the branching fractions, and the β parameters are presented and compared to the experimental results and the previous time-independent calculations.[17] The newly determined $\mathbf{a}_Q^{(K)}(p)$ parameters for $I(^2P_{3/2})$ and $I(^2P_{1/2})$ are discussed in Sec. III B and III C, respectively. The polarization of the corresponding H- and D-atom partners is presented in Sec. III D. Finally, some conclusions and proposals for experimental verification of these results are given in Sec. IV.

II. THEORY

In order to investigate photodissociation processes, knowledge of the underlying potential energy curves and the corresponding electronic transition dipole moments is required. In certain instances, one may also require the nonadiabatic couplings between the electronic states—they are not needed here as the dynamics are treated adiabatically without invoking coupling between the electronic states (see discussion below). Once the electronic structure is known, a methodology for treating the dynamics is required. We utilize a time-dependent wave packet treatment of the dynamics and from this we obtain the properties of interest, including the photofragmentation **T** matrix elements. Finally, the $\mathbf{a}_Q^{(K)}(p)$ parameters can be obtained from the photofragmentation **T** matrix elements using a well-established theoretical framework.[25,31–33] Since much of the theory has been presented elsewhere, we discuss each of these elements only briefly in so far as they apply to the photodissociation of HI.

A. Electronic structure

If spin-orbit coupling is not taken into account, the lowest energy asymptote for HI dissociation consists of $H(^2S)+I(^2P)$. These dissociation products correlate with four Λ-S electronic states, i.e., $X\,^1\Sigma^+$ (non degenerate), $a\,^3\Pi$ (sixfold degenerate), $A\,^1\Pi$ (doubly degenerate), and $t\,^3\Sigma$ (threefold degenerate). As in our previous studies of the hydrogen halides,[30,34–37] this is referred to as the diabatic basis. In the presence of the heavy iodine atom, there is a large spin-orbit interaction; the energy difference between the excited and ground spin-orbit states of iodine is $\Delta E = E(I\,^2P_{1/2}) - E(I\,^2P_{3/2}) = 7603.15\ cm^{-1}$.[38] The spin-orbit interaction acts as a coupling between the diabatic states. The fully adiabatic PECs can be determined from the diabatic curves and the spin-orbit couplings.[18] The 12 diabatic states transform into 12 adiabatic states upon diagonalization of the matrix containing (diagonal) diabatic energies and the (off-diagonal) spin-orbit coupling matrix elements. The adiabatic states are $X\,^1\Sigma_{0^+}$ (ground state), $A\,^1\Pi_1$ (two substates), $a\,^3\Pi_1$ (two substates), $t\,^3\Sigma_1$ (two substates), $a\,^3\Pi_2$ (two substates), $a\,^3\Pi_{0^+}$, $a\,^3\Pi_{0^-}$, and $t\,^3\Sigma_{0^-}$. The term symbols translate as a mixed Hund's case (a)/case (c) according to $^{2S+1}L_\Omega$. For Hund's case (c), Ω is the only good quantum number and the ^{2S+1}L labels designate the largest case (a) contribution within the Franck–Condon region, see Table III of Ref. 18. The case (a) and case (c) labels correspond to the diabatic and adiabatic representations, respectively.

While there have been several *ab initio* investigations of the electronic structure of HI,[18,20–22] in general, PECs and transition dipole moments have been produced by fitting to experimental data.[4,10,11,17,19,39,40] Except for in the work of

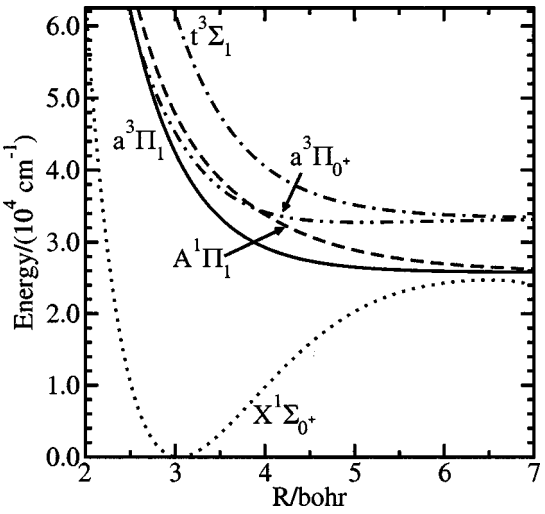

FIG. 1. The adiabatic potential energy curves as a function of the HI bond length as determined using the data from Ref. 17. All potential energies are for $J=0$. The potentials, in order of increasing energy in the asymptotic region, are $X\,^1\Sigma_{0^+}$ (dotted line), $a\,^3\Pi_1$ (solid line), $A\,^1\Pi_1$ (dashed line), $a\,^3\Pi_{0^+}$ (dot-dot-dash line), and $t\,^3\Sigma_1$ (dot-dash line).

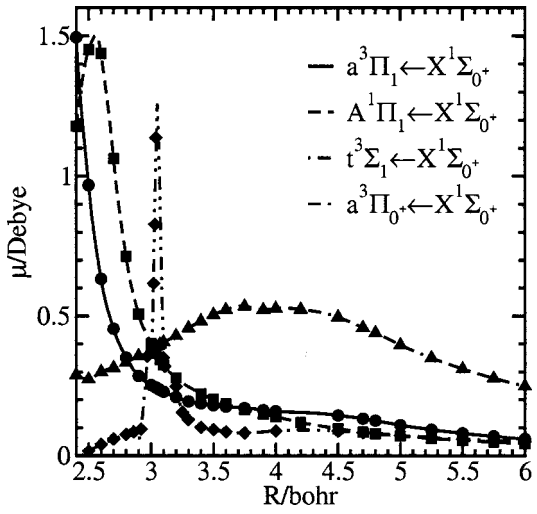

FIG. 2. Transition dipole moments as a function of HI bond length connecting the $X\,^1\Sigma_{0^+}$ ground electronic state and the $a\,^1\Pi_1$ (solid line), $A\,^1\Pi_1$ (dashed line), $a\,^3\Pi_{0^+}$ (dot-dot-dash line), and $t\,^3\Sigma_1$ (dot-dash line) excited electronic states. Data taken from Ref. 17 and represent the scaled *ab initio* data of Ref. 18.

Levy and Shapiro,[19] coupling between the electronic states has not been invoked in any of the fits; subsequently, it was shown that the β parameter measurements of van Veen *et al.*[12] which Levy and Shapiro fit were simply not correct. We choose to use the most recent PECs and associated transition dipole moments of LeRoy, Kraemer, and Manzhos.[17] Figure 1 illustrates the (adiabatic) potential energy curves, as determined in Ref. 17, involved in the photodissociation of HI in the *A* band, i.e., $X\,^1\Sigma_{0^+}$, $A\,^1\Pi_1$, $a\,^3\Pi_1$, $a\,^3\Pi_{0^+}$ and $t\,^3\Sigma_1$. The first three PECs correlate with the asymptote $H(^2S)+I(^2P_{3/2})$ while the latter two correlate with $H(^2S)+I(^2P_{1/2})$. The corresponding transition dipole moments are shown in Fig. 2. Rather than being from *ab initio* calculations, the PECs and transition dipole moments were determined by an empirical fit to the available experimental data [4–12] (total cross sections and I^* branching fractions) for both HI and DI. The *R* dependence of the transition dipole moments was guided by the *ab initio* results of Alekseyev *et al.*[18] It is particularly interesting to note the strong *R* dependence of the transition dipole moments. These PECs and transition dipole moments were then tested independently by demonstrating that they provide excellent values, as compared with experiment,[9,10] for the lowest order anisotropy parameter β. These functions were able to account for all of the experimental data for both isotopomers without any need to invoke coupling between the PECs.

In the fully adiabatic basis, the kinetic energy operator is formally no longer diagonal. Therefore, there are off-diagonal kinetic energy coupling terms (nonadiabatic couplings) of the form d^2/dR^2. However, the use of the fully adiabatic PECs is (most likely) justified in the case of HI. The potentials which can be coupled nonadiabatically are $A\,^1\Pi_1$, $a\,^3\Pi_1$, and $t\,^3\Sigma_1$. Also, the excited state $a\,^3\Pi_{0^+}$ can be coupled to the $X\,^1\Sigma_{0^+}$ ground state. There can not be coupling between states with different values of Ω (except for the negligibly small spin-rotation interaction[18]). Over most of the range of excitation energies considered, the $t\,^3\Sigma_1$ state is not energetically accessible and this state is well separated energetically from the other $\Omega=1$ states, see Fig. 1. Therefore, even if there is nonadiabatic coupling to this state from the $A\,^1\Pi_1$ and $a\,^3\Pi_1$ states, the probability of flux transfer to the $t\,^3\Sigma_1$ state is highly unlikely. Similarly, the energy difference between the $a\,^3\Pi_{0^+}$ and $X\,^1\Sigma_{0^+}$ states is large for all *R*, and thus flux transfer between these states due to nonadiabatic coupling is unlikely. The asymptotically degenerate $A\,^1\Pi_1$ and $a\,^3\Pi_1$ states could have nonadiabatic coupling between them but the available experiments measuring branching fractions and angular distributions can not distinguish between them. It is for these reasons that HI dissociation will be considered within a purely adiabatic model without coupling between any of the states, as was done by LeRoy, Kraemer, and Manzhos.[17]

The asymptotic ($R\rightarrow\infty$) energies of the molecular states and their corresponding wave functions can be determined using second-order perturbation theory.[41] The major contribution to the long-range energy is the van der Waals interaction. A detailed description of the correspondence to the adiabatic molecular states with particular atomic states is presented in Ref. 35 for the analogous HF molecule.

For the ground state $I(^2P_{3/2})$ fragment, the above adiabatic treatment implies that there are four states contributing to the angular distributions (orientation/alignment) of this fragment. The $a\,^3\Pi_1$ and $A\,^1\Pi_1$ states accessed through perpendicular excitation ($\Delta\Omega=\pm1$) correlate adiabatically as

$$HI(a\,^3\Pi_1;\Omega'=\pm1)\rightarrow H(m_H=\pm1/2)+I(m_I=\pm1/2) \tag{2}$$

and

$$HI(A\,^1\Pi_1;\Omega'=\pm1)\rightarrow H(m_H=\mp1/2)+I(m_I=\pm3/2). \tag{3}$$

In principle, the $X\,^1\Sigma_{0^+}$ state could gain population via nonadiabatic recoupling from the $a\,^3\Pi_{0^+}$ state. However, current

experimental measurements of β (Refs. 9 and 10) indicate that there is no parallel ($\Delta\Omega=0$) contribution to the production of $I(^2P_{3/2})$. Three excited states contribute to the angular distribution of the excited state $I(^2P_{1/2})$ fragment. The $a\ ^3\Pi_{0^+}$ state, which is accessed via a parallel ($\Delta\Omega=0$) transition, correlates equally with both $\pm 1/2\ m_H$ and $\mp 1/2\ m_{I^*}$ states, i.e.,

$$HI\left(^3\Pi_{0^+};\Omega'=0\right)\rightarrow H(m_H=\pm 1/2)+I^*(m_{I^*}=\mp 1/2). \tag{4}$$

The $t\ ^3\Sigma_1$ state, which is accessed via a perpendicular ($\Delta\Omega=0$) transition, correlates as

$$HI(t\ ^3\Sigma_1;\Omega'=\pm 1)\rightarrow H(m_H=\pm 1/2)+I^*(m_{I^*}=\pm 1/2). \tag{5}$$

The molecular wave functions corresponding to these asymptotes are given in Table II of Ref. 35. The long-range correlations given in Eqs. (2)–(5) are required for the determination of the orientation and alignment parameters $\mathbf{a}_Q^{(K)}(p)$, see Sec. II C.

B. Time-dependent wave packet dynamics

In the present work, we use a time-dependent wave packet formulation for the dynamics.[42–47] The time-dependent approach is based upon the solution of the nuclear Schrödinger equation

$$i\hbar\frac{\partial\Phi(R,t)}{\partial t}=\hat{H}(R)\Phi(R,t)=\left[-\frac{\hbar^2}{2\mu}\frac{d^2}{dR^2}+V(R)\right]\Phi(R,t), \tag{6}$$

where μ is the reduced mass of the system, $V(R)$ is a diagonal matrix of the adiabatic potential energies, and $\Phi(R,t)$ is a column vector describing the time-dependent wave function on each of the excited electronic states of the system. No off-diagonal (nonadiabatic) couplings are considered. Equation (6) also neglects the rotational part of the nuclear kinetic energy operator. As in our previous studies of hydrogen halide dissociation,[35–37,48] the axial recoil approximation is assumed to be valid, which is equivalent to neglect of the overall rotation of the molecule.

In the time-dependent approach, an initial wave packet $\phi_n(R,t=0)$, or, as is the case here, wave packets, is (are) prepared by taking the initial nuclear vibrational wave function of the molecule $\psi_{\Omega_i}(R)$ and multiplying it by the (adiabatic) transition dipole moment between the ground state and the n^{th} excited state $d^m_{q'}(R)$, i.e.,

$$\phi_n(R,t=0)=d^m_{q'}(R)\Psi_{\Omega_i}(R). \tag{7}$$

Here the index q' is the vector spherical harmonic component of the transition dipole moment function and it is determined by the symmetries of the ground and excited electronic states. For all calculations reported here, the initial ground state nuclear wave function corresponds to the $v=0$ vibrational state and has been determined using the Fourier grid Hamiltonian method.[42,49,50] Once the initial wave packets are defined, they are propagated in time under the influence of the excited state potential energy surfaces to provide the time dependent wave packets. The time propagation is performed using the Chebychev expansion technique.[51,52]

From our calculations, the three properties computed by LeRoy and co-workers[17,53] at 10 K are determined: the total cross section, the I^* branching fraction, and the β parameter. We briefly review the calculation of these properties from a time-dependent wave packet dynamics approach. As the wave packets move towards the asymptotic large R region, they are analyzed at each time step as they pass through an analysis line defined at a large fixed value of R ($=R_\infty$). Energy dependent coefficients[36,37,43] $A_n(R_\infty,E)$ are then obtained by taking the Fourier transform over time of these cuts through the time-dependent wave packets $\phi_n(R_\infty,t)$, i.e.,

$$A_n(R_\infty,E)=\frac{1}{2\pi}\int_0^\infty \phi_n(R_\infty,t)\exp[i(E_i+h\nu)t/\hbar]dt. \tag{8}$$

The partial absorption cross sections can be written in terms of these coefficients

$$\sigma_n(\nu)=\frac{32\pi^3\nu k_\nu}{3c\epsilon_0}|A_n(R_\infty,E)|^2, \tag{9}$$

where k_v is the asymptotic wave vector for this channel. The total cross section is determined as the sum over all of the partial cross section

$$\sigma_{\text{tot}}(\nu)=\sum_{i=1}^{4} g_n\sigma_n(\nu), \tag{10}$$

where g_n is a degeneracy factor equal to 2, 2, 1, and 2 for the $A\ ^1\Pi_1$, $a\ ^3\Pi_1$, $a\ ^3\Pi_{0^+}$, and $t\ ^3\Sigma_1$ states, respectively. The total cross section is related to the molar absorption coefficient by $\varepsilon=10N_A\sigma/\ln 10$, where N_A is the Avogadro constant.

The branching fraction is the ratio between I^* production and the total amount of atomic iodine produced and is given by

$$\Gamma=\frac{\sigma_{I^*}}{\sigma_{\text{tot}}}=\frac{\sigma_{^3\Pi_{0^+}}+g_{^3\Sigma_1}\sigma_{^3\Sigma_1}}{\sigma_{\text{tot}}}. \tag{11}$$

The branching fraction is also referred to as the quantum yield. Note that the branching *fraction* calculated here is different from the branching *ratio* given by σ_{I^*}/σ_I which is reported elsewhere, e.g., Refs. 9–12 and 19.

Since the photodissociation is direct, the lowest order anisotropy parameter β can also be determined from the partial photodissociation cross sections. The β parameter for the production of I^* is of most interest and is given by

$$\beta=\frac{2\sigma_{^3\Pi_{0^+}}-g_{^3\Sigma_1}\sigma_{^3\Sigma_1}}{\sigma_{I^*}}, \tag{12}$$

where $\sigma_{I^*}=\sigma_{^3\Pi_{0^+}}+g_{^3\Sigma_1}\sigma_{^3\Sigma_1}$ is the total cross section leading to the production of excited state iodine fragments. According to this equation, a purely parallel transition corresponds to $\beta=2$ while a purely perpendicular transition corresponds to $\beta=-1$. The excellent agreement of these results, Eqs. (10)–(12), with LeRoy's low temperature results[17] and with experiment (see Sec. III A) establishes the veracity of our time-dependent wave packet computations, which neglect ro-

tation, and will allow the prediction of the anisotropy parameters $\mathbf{a}_Q^{(K)}(p)$ for a low temperature experiment.

C. Determination of dynamical functions and $\mathbf{a}_Q^{(K)}(p)$ parameters

While the scalar and the lowest order vector properties are of interest, we want to determine a set of parameters describing the orientation and alignment of the atomic fragments. The theoretical and/or experimental determination of these parameters provides the most detailed understanding of the photodissociation dynamics. For a photofragment with angular momentum j, the magnitude of these distinct spatial distributions (in the molecular frame) can be fully described by the $\mathbf{a}_Q^{(K)}(p)$ parameters. K and Q refer to the spatial distribution in the molecular frame and p refers to the symmetry of the transition connecting the ground electronic state to the dissociative excited states. The symmetry p can be pure perpendicular ($\perp$), pure parallel ($\parallel$), or mixed parallel/perpendicular ($\parallel$, $\perp$). The dimensionless anisotropy parameters $\mathbf{a}_Q^{(K)}(p)$ are normalized combinations of the dynamical functions $f_K(q,q')$ (see discussion below). Note that an alternate set of anisotropy parameters related to the laboratory frame have also been presented.[31,54]

The relevant dynamical functions for a photofragment with angular momentum j_A range from $K=0$ to $K=2j_A$,[55,56] where K is referred to as the multipole rank. The terminology "multipole rank" is used as the dynamical functions are directly related to the angular momentum state multipoles $\rho_{KQ}^{j_A}(\theta,\phi)$, see Eq. (5) of Ref. 35. For the ground state iodine fragment ($j_A=3/2$), the complete set of state multipoles (dynamical functions) contains $K=0$ (population), $K=1$ (orientation, dipole moment), $K=2$ (alignment, quadrupole moment), and $K=3$ (orientation, octupole moment). The description for the excited state iodine fragment ($j_A=1/2$) requires only $K=0$ and $K=1$ dynamical functions. Similarly, the hydrogen atom fragment ($j_B=1/2$) resulting from the photolysis can be described using state multipoles (dynamical functions) of rank $K=0$ and $K=1$ only.

For a diatomic molecule AB dissociating into atoms A and B having angular momenta j_A and j_B, respectively, the dynamical functions for fragments A are defined as

$$f_K(q,q') = \sum_{n,\Omega,\Omega_A,n',\Omega',\Omega_A'} (-1)^{K+j_A+\Omega_A'} \times \begin{pmatrix} j_A & j_A & K \\ -\Omega_A & \Omega_A' & q-q' \end{pmatrix} T^{n\Omega}_{j_A\Omega_A j_B\Omega_B} (T^{n'\Omega'}_{j_A\Omega_A' j_B\Omega_B})^* \times \langle \Psi^-_{n,\Omega}(R,E)|\hat{\mathbf{d}}_q|\Psi_{\Omega_i}\rangle^* \langle \Psi^-_{n',\Omega'}(R,E)|\hat{\mathbf{d}}_{q'}|\Psi_{\Omega_i}\rangle. \tag{13}$$

The expression $\langle \Psi^-_{n,\Omega}(R,E)|\hat{\mathbf{d}}_q|\Psi_{\Omega_i}\rangle$ is the energy-dependent photofragmentation $\mathbf{T}$ matrix element associated with channel n, and has been shown previously[35,43] to be given by

$$\langle \Psi^-_{n,\Omega}(R,E)|\hat{\mathbf{d}}_q|\Psi_{\Omega_i}\rangle = i\left(\frac{h^2k_v}{2\pi\mu}\right)^{1/2} \exp(-ik_vR_\infty)A_n(R_\infty,E). \tag{14}$$

$A_n(R_\infty,E)$ appearing in Eq. (14) are the energy-dependent coefficients obtained from the time-dependent dynamics calculation [see Eq. (8)]. In Eq. (13), the indices q and q' are the vector spherical harmonic components[56,57] of the molecular electric dipole moment with respect to the recoil axis. They can take only the values 0 or ±1, corresponding to parallel or perpendicular electronic transitions, respectively. The initial and final z components of the total electronic angular momentum about the molecular axis are related by $\Omega=\Omega_i+q$. The diagonal elements of the dynamical functions $f_K(q,q')$ with $q=q'$ correspond to incoherent excitation of parallel, or perpendicular transitions, while the off-diagonal elements with $q\neq q'$ correspond to coherent excitation of different molecular continua. The expression for the dynamical functions of fragments B can be obtained from Eq. (13) by exchanging subscripts A and B.

As discussed above, parameters up to ranks $K=3$ and $K=1$ are utilized for describing the ground state iodine I($^2P_{3/2}$) and the excited state iodine I($^2P_{1/2}$) fragments, respectively, resulting from HI photodissociation. The zeroth-rank anisotropy parameter is the well-known β parameter, see also Eq. (12). In terms of the $K=0$ dynamical functions, β is given as[31]

$$\beta = \frac{2[f_0(0,0)-f_0(1,1)]}{2f_0(1,1)+f_0(0,0)}. \tag{15}$$

Note that β has been determined previously for HI and DI using Eq. (12).[17] Of course, Eqs. (15) and (12) can be shown to be formally equivalent.

The newly computed anisotropy parameters discussed in Sec. III include three parameters describing incoherent perpendicular excitation $\mathbf{a}_0^{(1)}(\perp)$, $\mathbf{a}_0^{(2)}(\perp)$, and $\mathbf{a}_0^{(3)}(\perp)$, two parameters describing coherent perpendicular excitation $\mathbf{a}_2^{(2)}(\perp)$ and $\mathbf{a}_2^{(3)}(\perp)$, and a single parameter describing coherent parallel and perpendicular excitation $\mathbf{a}_1^{(1)}(\parallel,\perp)$. In principle, there are additional parameters describing coherent parallel and perpendicular excitations for the production of ground state iodine, i.e., $\mathbf{a}_Q^{(K)}(\parallel,\perp)$, $2\leqslant K\leqslant 3$. However, within the present adiabatic treatment of the dynamics, there is no parallel contribution to I($^2P_{3/2}$) fragments and therefore all $\mathbf{a}_Q^{(K)}(\parallel,\perp)$ parameters are identically zero. Only a single state accessed by parallel excitation correlates with each asymptote, and thus no parallel only parameters $\mathbf{a}_Q^{(K)}(\parallel)$ are computed.

The parameters describing incoherent perpendicular excitation are related to the dynamical functions, Eq. (13) by

$$\mathbf{a}_0^{(1)}(\perp) = \frac{f_1(1,1)}{f_0(1,1)}, \tag{16}$$

$$\mathbf{a}_0^{(2)}(\perp) = V_2(j_I)^{-1}\frac{f_2(1,1)}{f_0(1,1)}, \tag{17}$$

and

$$\mathbf{a}_0^{(3)}(\perp) = V_3(j_I)^{-1}\frac{f_3(1,1)}{f_0(1,1)}. \tag{18}$$

For the ground state iodine photofragment, the parameters $V_2(j_I)$ and $V_3(j_I)$ are given by

$$V_2(j_I = 3/2) = \left[\frac{j_I(j_I+1)}{(2j_I+3)(2j_I-1)}\right]^{1/2} = \frac{\sqrt{15}}{4\sqrt{3}} \tag{19}$$

and

$$V_3(j_I = 3/2) = \frac{j_I(j_I+1)}{[(j_I-1)(j_I+2)(2j_I-1)(2j_I+3)]^{1/2}} = \frac{15}{4\sqrt{21}}. \tag{20}$$

Recall that only the $\mathbf{a}_0^{(1)}(\perp)$ parameter is required for the description of the excited state iodine fragment.

The description of the angular distribution of the ground state I($^2P_{3/2}$) fragment also requires two parameters for coherent perpendicular excitation, i.e.,

$$\mathbf{a}_2^{(2)}(\perp) = -\frac{1}{2}V_2(j_I)^{-1}\frac{f_2(1,-1)}{f_0(1,1)} \tag{21}$$

and

$$\mathbf{a}_2^{(3)}(\perp) = \frac{i}{2}V_3(j_I)^{-1}\frac{f_3(1,-1)}{f_0(1,1)}. \tag{22}$$

For the excited state iodine fragment, the parameter $\mathbf{a}_1^{(1)}(\parallel, \perp)$ describing coherent parallel and perpendicular excitation is

$$\mathbf{a}_1^{(1)}(\parallel, \perp) = \frac{-3\sqrt{2}f_1(1,0)}{2f_0(1,1) + f_0(0,0)}. \tag{23}$$

The parameter describing coherent parallel and perpendicular excitation usually has its real and imaginary parts presented separately.[32]

In the above description of the anisotropy parameters, the nuclear spins of the photofragments have been neglected. This assumption is justified since the duration of the dissociation process is typically much smaller than the Heisenberg uncertainty time, $\Delta t = \hbar/(2\Delta E)$, associated with the hyperfine splitting in the atoms. While the nuclear spins do not affect the photodissociation dynamics, the hyperfine interaction in the final fragments is important as it results in partial depolarization of the fragment's electron angular momenta.[56] For the dissociation of the HI molecule considered here, any orbital alignment of the I atom photofragment will degrade to $\approx$23% of its nascent value through coupling with the I=5/2 nuclear spin.

III. RESULTS AND DISCUSSION

A. Cross sections, branching fractions, and β parameters

Using the time-dependent wave packet approach outlined in Sec. II B, the scalar properties and the lowest anisotropy parameter β are computed in order to compare with the time-independent results of LeRoy, Kraemer, and Manzhos.[17] These calculations are performed to verify that our calculations, which assume excitation from $v=0$ and neglect rotation, are in good accord with the previous results, which include Boltzmann averages over vibrational and rotational levels. Also, these properties will prove useful in guiding the discussion and elucidating the importance of the higher order anisotropy parameters in providing new insight into the dynamics and for testing the current model[17] of the dynamics.

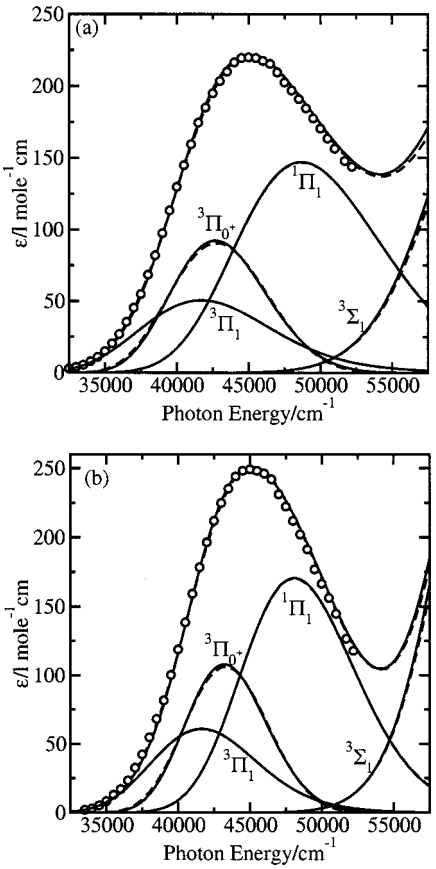

FIG. 3. The total and partial absorption coefficients for the photodissociation of (a) HI and (b) DI. Results are from the present time-dependent wave packet calculations (solid lines), the time-independent calculations of Ref. 17 (dashed lines), and the experimental measurements of Ref. 4 (○).

Figure 3 illustrates the total molar absorption coefficient, as well as the partial cross sections due to the four excited electronic states, as a function of photolysis energy for both HI and DI. Also, shown for comparison are the calculations of LeRoy and co-workers[17,53] at 10 K (the Boltzmann averages included vibrational and rotational states $v \leqslant 1$, $J \leqslant 3$ for HI and $v \leqslant 1$, $J \leqslant 4$ for DI) and the experimental measurements at 300 K.[4] The experimental results for DI represent the scaled, $\varepsilon_{\text{scaled}} = \varepsilon/0.9694$, results of Ref. 17. The slight discrepancy between our results and Leroy's at high energy is most likely due to the fact that our calculations are for rotationless v=0 molecules while Leroy's results represent Boltzmann averages; comparison with Leroy's results[53] at 10, 300, and 1000 K indicate that the high energy discrepancy increases as a function of increasing temperature. The intensity maximum associated with excitation into the $t\,^3\Sigma_1$ state is not discerned by the experimental measurements presented here; the theoretical maximum based on the present

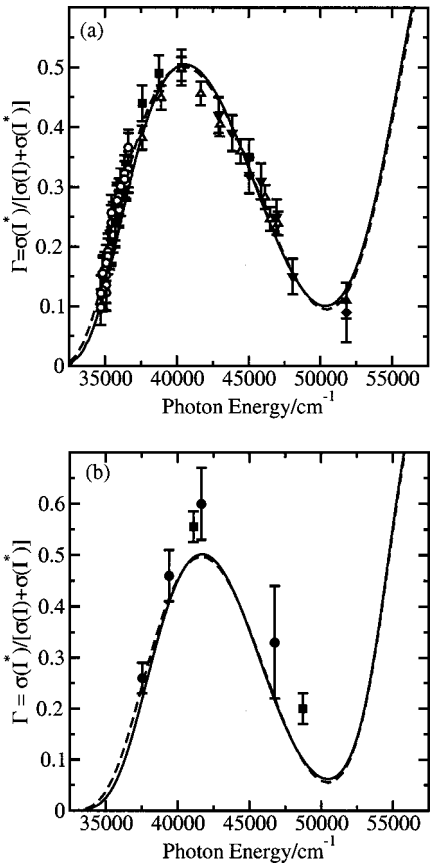

FIG. 4. The I atom excited state branching fraction, Eq. (10), as function of photon energy for the photodissociation of (a) HI and (b) DI. Results are from the present time-dependent wave packet calculations (solid lines), the time-independent calculations (Ref. 17) at 10 K (dashed lines), and the experimental measurements for HI (Refs. 5–12) and DI (Refs. 7 and 11).

PECs and transition dipole moments occurs at 61 982 cm^{-1}. For $\nu \geqslant 55\,600$ cm^{-1}, the absorption spectrum exhibits structure due to absorption into various excited bound states lying above the valence states discussed in Sec. II A.[1–3,40] Therefore, the predictions for the anisotropy parameters for the ground and excited state iodine atoms should be valid for nearly the entire energy range presented (32 500–55 000 cm^{-1}) since the $A\,^1\Pi_1$, $a\,^3\Pi_1$, $a\,^3\Pi_{0^+}$, and $t\,^3\Sigma_1$ states are the only ones contributing to absorption in this energy region.

The calculated branching fractions, see Eq. (11), for both HI and DI as a function of excitation energy are illustrated in Fig. 4. The present results are for excitation from $v=0$. Also displayed are the results from the previous time-independent calculations[17] and the experimental results.[5–11]

The anisotropy parameter for the I and I* channels are shown in Fig. 5 as a function of excitation frequency. Results are only shown for the dissociation of HI—as with the total cross sections and the branching fractions, the results for DI are extremely similar. Also illustrated are the previous calculations[17] based on these potentials and transition dipole moments, as well as the most recent experimental measurements.[9,10] The I atom products result exclusively from the perpendicular transitions to the $a\,^3\Pi_1$ and the $A\,^1\Pi_1$ states in agreement with all previous experimental measurements[9,11,12,14] and the original interpretation by

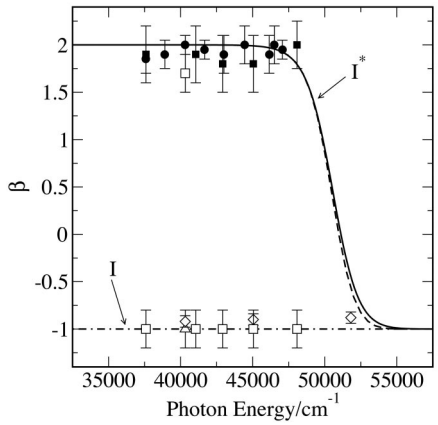

FIG. 5. The anisotropy distribution parameter β as a function of photon energy for the I* and I atoms resulting from the photodissociation of HI. Results are from the present time-dependent wave packet calculations (solid and dotted lines for I* and I respectively), the time-independent calculations at 10 K of Ref. 17 (dashed and dash-dot lines), and the experimental measurements of Langford *et al.* (Ref. 9) (■ and □), Gendron and Hepburn (Ref. 10) (●), van Veen (Ref. 12) ◇, and Xu, Koplitz, and Wittig (Ref. 14) (△). Time-dependent and time-independent results are indistinguishable for the ground state I fragment.

Mulliken.[16] For I*, the situation is fairly clear, namely, that it results primarily from the parallel $a\,^3\Pi_{0^+} \leftarrow X\,^1\Sigma_{0^+}$ transition below 50 000 cm^{-1} and from the perpendicular transition above 50 000 cm^{-1}. However, the extent of a perpendicular contribution (if any) in the low energy region is still open. Based on measurements at 208.0, 222, 233, 243.6, 248, and 266 nm (37 594–48 077 cm^{-1}), Langford[9] and Wittig[14] suggest 7%–10% of I* arises from perpendicular transitions, while Gendron[10] suggests that in this energy region I* results from a purely parallel transition. LeRoy's analysis shows that I* is obtained from purely parallel transitions below 46 000 cm^{-1} and purely perpendicular transitions above 55 000 cm^{-1} and this successfully models all of the experimental data within experimental error bars. In fact, LeRoy suggests[17] "measurements of the quantum yield and the I* photofragment anisotropy distribution at frequencies $\geqslant$50 000 cm^{-1} would provide a sharp test of the present model."

In the following sections, we focus on the determination of the higher order anisotropy parameters $\mathbf{a}_Q^{(K)}(p)$ (within the current adiabatic model for dissociation) and suggest how their measurement can confirm or discredit the current model. In particular, higher order parameters must be examined to determine the relative roles of the $a\,^3\Pi_1$ and $A\,^1\Pi_1$ states. These states can not be distinguished via measurement of either the I* branching fraction, since both correlate with ground state fragments, or the β parameter, since both are accessed via perpendicular transitions. We also demonstrate the sensitivity of the $\mathbf{a}_1^{(1)}(\parallel, \perp)$ parameter to the relative amounts of parallel and perpendicular excitation.

B. Anisotropy parameters for I($^2P_{3/2}$)

The angular distribution for the ground state iodine fragment I($^2P_{3/2}$) is described by anisotropy parameters up to rank $K=3$. When dissociating with linearly polarized light,

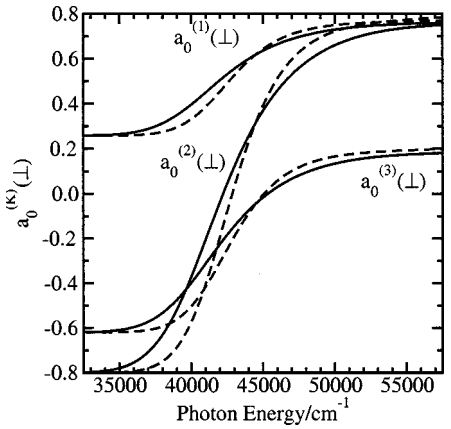

FIG. 6. Incoherent anisotropy parameters $\mathbf{a}_0^{(K)}(\perp)$ for the production of ground state I($^2P_{3/2}$) as a function of photon energy for the photodissociation of HI (solid lines) and DI (dashed lines) initially in their rotationless ground, $v=0$, vibrational states.

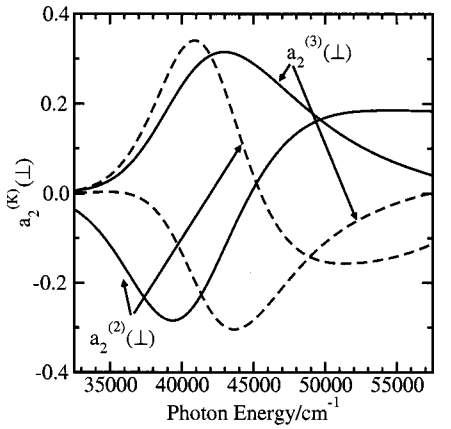

FIG. 7. Coherent anisotropy parameters $\mathbf{a}_2^{(K)}(\perp)$ for the production of ground state I($^2P_{3/2}$) as a function of photon energy for the photodissociation of HI (solid lines) and DI (dashed lines) initially in their rotationless ground, $v=0$, vibrational states.

the spatial distribution $D_\perp(\theta,\phi)$ of the angular momentum of an ensemble of photofragments from a pure perpendicular transition is[32]

$$D_\perp(\theta,\phi) = 1 + a_0^{(2)}(\perp)P_2(\cos\theta) + a_2^{(2)}(\perp)\sin^2\theta\cos 2\phi. \tag{24}$$

As discussed in Sec. II A, the I($^2P_{3/2}$) fragments arise from a pure perpendicular transition within the current adiabatic model of dissociation. The angular distribution of the iodine photofragments is only sensitive to the odd K anisotropy parameters when dissociating with circularly polarized light.[32]

Figure 6 illustrates the anisotropy parameters describing incoherent perpendicular excitation $\mathbf{a}_0^{(K)}(\perp)$ for the ground state I($^2P_{3/2}$) fragment produced from the photodissociation of HI and isotopically substituted DI as a function of photolysis wavelength. The results are for excitation from the rotationless ground $v=0$ vibrational state. The theoretical results for I($^2P_{3/2}$) produced from photodissociating HI and DI at 193 nm are presented in Table I The values for photodissociation by 193 nm light are given since this is an experimentally convenient wavelength and it lies in the interesting spectral region (50 000–55 000 cm^{-1}) as suggested by LeRoy.[17] Figure 6 shows that there are significant similarities in the behavior of the $\mathbf{a}_0^{(K)}(\perp)$ parameters as a function of photolysis frequency for the I($^2P_{3/2}$) produced from HI and DI. In fact, these differences are less than or equal to the typical error bars associated with the experimental measurement of $\mathbf{a}_0^{(K)}(\perp)$ parameters. These results are in marked contrast to those for HCl and DCl photodissociation,[34] where the Cl ($^2P_{3/2}$) produced from HCl is strongly aligned [cf., $\mathbf{a}_0^{(2)}(\perp)$], while that produced from DCl exhibits essentially no alignment, i.e., $\mathbf{a}_0^{(2)}(\perp)\approx 0$.

TABLE I. Theoretical alignment and orientation parameters for I($^2P_{3/2}$) fragments produced from HI and DI dissociation at 193 nm (51 813 cm^{-1}). Also given is the allowed range for each parameter. $\mathbf{a}_1^{(1)}(\parallel,\perp)$ parameters are zero within the current adiabatic model of dissociation.

	HI	DI	Range
$\mathbf{a}_0^{(1)}(\perp)$	0.74	0.76	±0.775
$\mathbf{a}_0^{(2)}(\perp)$	0.70	0.75	±0.800
$\mathbf{a}_0^{(3)}(\perp)$	0.16	0.18	±0.207
$\mathbf{a}_2^{(2)}(\perp)$	0.18	−0.16	±0.566
$\mathbf{a}_2^{(3)}(\perp)$	0.12	−0.07	±0.327
β	−1.0	−1.0	−1.0,…,2.0

The $\mathbf{a}_2^{(K)}(\perp)$ parameters describing the coherent perpendicular excitation of the $a\ ^3\Pi_1$ and $A\ ^1\Pi_1$ states are illustrated in Fig. 7 for the I($^2P_{3/2}$) fragment arising from the photodissociation of HI and DI from $v=0$. The $\mathbf{a}_2^{(2)}(\perp)$ parameter describes the degree of coherence between pairs of m states, m and $m\pm 2$. The large values of $\mathbf{a}_2^{(2)}(\perp)$ indicate that the photofragment angular distributions are not cylindrically symmetric with respect to the recoil direction, see Eq. (24). The theoretically determined parameters depend strongly on photolysis energy over the entire energy range. Unlike what is seen for the $\mathbf{a}_0^{(K)}(\perp)$ parameters, there are fairly significant differences between the $\mathbf{a}_2^{(K)}(\perp)$ parameters for HI and DI Within the adiabatic model for dissociation, the magnitude of the $\mathbf{a}_2^{(K)}(\perp)$ parameters is related to the relative probability of excitation into the $a\ ^3\Pi_1$ or $A\ ^1\Pi_1$ excited states. As such for any fixed value of the photolysis energy, the magnitudes are comparable for both HI and DI (especially if one accounts for the decrease in zero-point energy for DI). On the other hand, the sign of the $\mathbf{a}_2^{(K)}(\perp)$ parameters depends on the phase difference between the photofragmentation **T** matrix elements for the $a\ ^3\Pi_1$ and $A\ ^1\Pi_1$ states. Therefore, it is interesting that the $\mathbf{a}_2^{(K)}(\perp)$ parameters are of opposite signs for HI and DI. The calculated difference awaits experimental verification and, if verified, will provide additional confirmation of the current model of adiabatic photodissociation for HI.[17] In particular, it will provide information strongly sensitive to the details of the $a\ ^3\Pi_1$ and $A\ ^1\Pi_1$ excited electronic states including possible nonadiabatic coupling.

As discussed in Sec. II C in principle, $\mathbf{a}_1^{(1)}(\parallel,\perp)$ parameters describing coherent parallel and perpendicular excitations could be needed to define completely the angular distribution of I($^2P_{3/2}$). Neglecting spin-rotation interaction, the parallel component could only arise through nonadiabatic coupling of the $a\ ^3\Pi_{0+}$ and $X\ ^1\Sigma_{0+}$ states, see discussion for

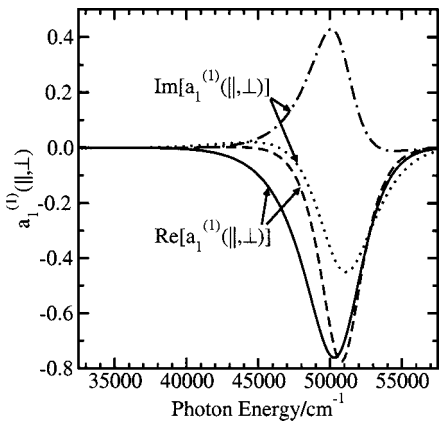

FIG. 8. Coherent anisotropy parameters $\mathrm{Re}[\mathbf{a}_1^{(1)}(\parallel,\perp)]$ and $\mathrm{Im}[\mathbf{a}_1^{(1)}(\parallel,\perp)]$ for the production of excited state $I(^2P_{1/2})$ as a function of photon energy for the photodissociation of HI (solid and dotted lines) and DI (dashed and dot-dash lines) initially in their rotationless ground, $v=0$, vibrational states.

HCl[34] Any experimentally measured deviation of the $\mathbf{a}_1^{(1)}(\parallel,\perp)$ from zero would indicate a minor parallel component; as discussed by Rakitzis and Zare[32] the $\mathbf{a}_Q^{(1)}(\parallel,\perp)$ parameters for $|Q|=1$ are extremely sensitive to the simultaneous presence of states of parallel and perpendicular symmetry. However, experimental measurements[9,11,12,14] of the lowest order anisotropy parameter β seem to indicate that only perpendicular transitions contribute to the $I(^2P_{3/2})$ products.

C. Anisotropy parameters for $I(^2P_{1/2})$

The excited state $I(^2P_{1/2})$ fragment's angular distribution is fully described by orientation ($K=1$) parameters only, unlike the angular distribution of $I(^2P_{3/2})$ which requires both orientation ($K=1$ and $K=3$) and alignment ($K=2$) parameters.

The $\mathbf{a}_0^{(1)}(\perp)$parameter describing $I(^2P_{1/2})$ production is not plotted as it is equal to the maximal value of 0.577 ($=1/\sqrt{3}$), independent of photolysis energy, for both HI and DI. This parameter exhibits no energy dependence since only a single state ($^3\Sigma_{\Omega=+1}$ or $^3\Sigma_{\Omega=-1}$) contributes to the photofragmentation cross section; the particular state involved depends upon whether right- or left-circularly polarized light is utilized in the dissociation.[30] On the other hand, the $\mathrm{Re}[\mathbf{a}_1^{(1)}(\parallel,\perp)]$ and $\mathrm{Im}[\mathbf{a}_1^{(1)}(\parallel,\perp)]$ parameters describing coherent parallel and perpendicular excitation do show a strong photolysis energy dependence in the region where excitation to both $a\,^3\Pi_{0^+}$ and $t\,^3\Sigma_1$ are feasible, i.e., $\approx$41 000–56 000 cm^{-1}, see Fig. 8. Note that the $\mathbf{a}_1^{(1)}(\parallel,\perp)$ parameters are much more sensitive to the amount of parallel and perpendicular excitation than the corresponding β parameters, see Fig. 5. While the $\mathrm{Re}[\mathbf{a}_1^{(1)}(\parallel,\perp)]$ parameters for $I(^2P_{1/2})$ produced from HI and DI are similar across the entire energy range illustrated, the calculated $\mathrm{Im}[\mathbf{a}_1^{(1)}(\parallel,\perp)]$ parameters from HI and DI exhibit opposite signs. The difference between $\mathrm{Im}[\mathbf{a}_1^{(1)}(\parallel,\perp)]$ parameters for HI and DI could be measured experimentally and Table II presents the theoretical results for $I(^2P_{1/2})$ produced from dissociating HI and DI at 193 nm.

TABLE II. Theoretical alignment and orientation parameters for $I(^2P_{1/2})$ fragments produced from HI and DI dissociation at 193 nm (51 813 cm^{-1}). Also given is the allowed range for each parameter.

	HI	DI	Range
$\mathbf{a}_0^{(1)}(\perp)$[a]	0.58	0.58	$\pm$0.577
$\mathrm{Re}[\mathbf{a}_1^{(1)}(\parallel,\perp)]$	−0.54	−0.56	$\pm$0.866
$\mathrm{Im}[\mathbf{a}_1^{(1)}(\parallel,\perp)]$	−0.41	+0.15	$\pm$0.866
β	−0.44	−0.60	−1.0,…,2.0

[a]This is equal to the maximal value of $1/\sqrt{3}$ independent of photolysis energy (see text).

The $\mathrm{Im}[\mathbf{a}_1^{(1)}(\parallel,\perp)]$ parameter is dependent on the sine of the phase difference of the radial wave functions created on the $a\,^3\Pi_{0^+}$ and $t\,^3\Sigma_1$ states, i.e., $\sin\Delta\phi$, modulated by the transition amplitudes for these transitions.[31,32] On the other hand, the $\mathrm{Re}[\mathbf{a}_1^{(1)}(\parallel,\perp)]$ parameter has a $\cos\Delta\phi$ dependence. Therefore, the difference between HI and DI reflect these differences and measurement of the $\mathbf{a}_1^{(1)}(\perp)$ parameters will provide detailed information regarding the $a\,^3\Pi_{0^+}$ and $t\,^3\Sigma_1$ states. Due to the sensitivity of $\mathbf{a}_1^{(1)}(\parallel,\perp)$ relative to β, experimental measurements below $\approx$45 000 cm^{-1} should be able to provide evidence for or against the possibility of nonadiabatic coupling between the $t\,^3\Sigma_1$ state and the $a\,^3\Pi_1$ and $A\,^1\Pi_1$states. It is clear that direct excitation to $t\,^3\Sigma_1$ is not feasible in that energy range,[18] see Fig. 1, and therefore, any perpendicular contribution to the I^* dissociation channel must be from nonadiabatic coupling.

D. H/D atom polarization

Due to the small excited state spin-orbit splitting that must be resolved for the hydrogen atom in a laser ionization experiment, spin orientation of the hydrogen atom is extremely difficult to measure using that technique.[58,59] While the alignment/orientation of the iodine atom is much more easily measured than that of the H atom, the polarization of the H atom can be readily computed. The polarization of the H atom can be inferred from experimental measurement of the angular momentum distributions of the ground and excited state iodine atoms.

The angular dependence of the H atom (H electron) spin polarization is the difference in the population of the spin-up and spin-down states normalized to their sum,

$$P_e(\theta_c)=\frac{(n_+-n_-)}{(n_++n_-)}. \tag{25}$$

By utilizing the long-range correlations, see Eqs. (2)–(5), the partial cross sections, and Eq. (25), we can readily determine the H atom spin polarization.

Equation (25) describes the electron spin polarization for the time after photodissociation that is much shorter than the hyperfine interaction precession period in the H atom ($\tau_{\mathrm{hf}}=0.7$ ns). For longer times, the electron and proton angular momenta are coupled by the nuclear hyperfine interaction, and therefore after the dissociation, the polarization oscillates between the two. In the long-time limit, $t\gg\tau_{\mathrm{hf}}$, the right-hand side of Eq. (25) should be multiplied by the depolarization factor 1/2.

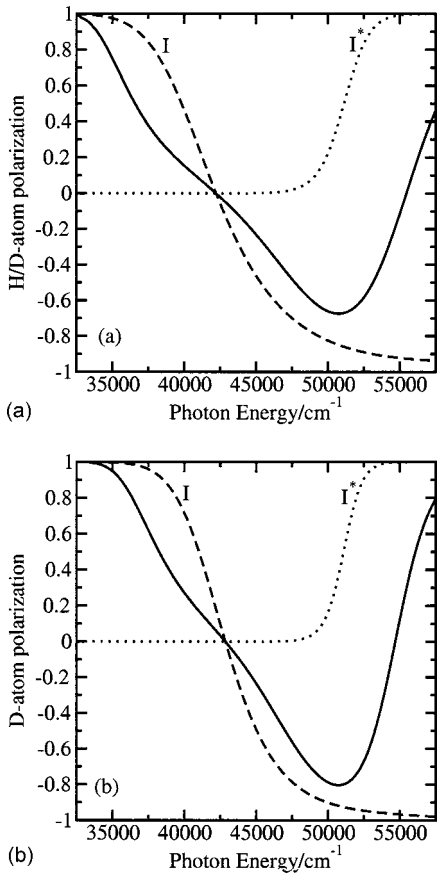

FIG. 9. H/D atom polarization as a function of photon energy for the photodissociation of (a) HI and (b) DI initially in their rotationless ground, $v=0$, vibrational states. In each panel, three results are illustrated: H/D atoms produced with I($^2P_{3/2}$) partners (dashed line), with I($^2P_{1/2}$) partners (dotted line), and the weighted average (solid line).

Rather than plotting the $\mathbf{a}_1^{(1)}(\parallel,\perp)$ and $\mathbf{a}_0^{(1)}(\perp)$ parameters for the H atom (recall $K\leqslant 1$ since $j=1/2$), we present in Figs. 9(a) and 9(b) the maximum polarization degree P_e for H atoms (D atoms) produced with I and I* cofragments and the weighted average, see Eqs. (2)–(6). If we consider H/D produced with I($^2P_{3/2}$) partners, i.e., "fast" H/D atoms, then highly spin polarized, i.e., $P_e>50\%$, hydrogen (deuterium) atoms can be produced for energies below 40 000 cm^{-1} and above 45 000 cm^{-1}; the H atoms are spin polarized in opposite senses in these two energy regimes. The change in spin polarization reflects the change in absorption from the $a\,^3\Pi_1$ state being dominant at low energies to the $A\,^1\Pi_1$ state being dominant at higher energies, see Fig. 3 and Eqs. (2) and (3). On the other hand, for "slow" H/D atoms correlating with excited state iodine products, there is no spin polarization for energies less than 47 500 cm^{-1} but highly spin polarized H/D atoms for energies greater than 51 000 cm^{-1}. This behavior reflects the relative contributions of the $a\,^3\Pi_{0^+}$ and the $t\,^3\Sigma_1$ states, see Fig. 3 and Eqs. (4) and (5). Therefore, if we consider all H/D atoms produced, highly spin polarized hydrogen atoms (SPH) can be produced for excitation energies below 37 500 cm^{-1} and between 47 500 and 52 500 cm^{-1}. Also, highly spin polarized deuterium atoms (SPD) can be produced for these same energy ranges. The calculations show that there is a high degree of spin polarization for D atoms produced from excitation energies greater than 55 000 cm^{-1}. However, at these energies other excited electronic states begin to contribute to the absorption[3] and thus predictions based on the current model are probably not appropriate. The prediction of both spin polarized hydrogen and deuterium atoms from the photodissociation of HI and DI stands in marked contrast to the photodissociation of HCl and DCl where highly SPH can be produced for excitation energies below 55 000 cm^{-1}, while the dissociation of DCl does not produce highly spin polarized D atoms at any frequency.

Experimentally, right- or left-circularly polarized light can be used to select $\Omega'=+1$ or -1, respectively, parallel to the light propagation direction, in order to produce SPH (or SPD). For laser pulses much shorter than 0.7 ns, the polarization plotted in Fig. 9 can be selected for either electron or proton. For laser pulses longer than 0.7 ns, the polarization of both the electron and the proton will be averaged, i.e., half of the plotted value.

IV. CONCLUSIONS

We have examined the photodissociation of HI and DI using time-dependent wave packet dynamics. Not surprisingly, the scalar properties σ and Γ agree with the time-independent results of LeRoy, Kraemer, and Manzhos.[17] Of course, the results also then agree with the experimental measurements which were used to fit the empirical PECs and transition dipole moments. Most importantly, the paper presents the *ab initio* calculation of the (near) complete set of anisotropy parameters $\mathbf{a}_Q^{(K)}(p)$ describing the I($^2P_{3/2}$) and I($^2P_{1/2}$) angular momentum distributions arising from the photodissociation of HI and DI as a function of photon energy.[60]

The anisotropy parameters as a function of photolysis wavelength for HI and DI have been compared. The $\mathbf{a}_0^{(K)}(p)$ anisotropy parameters for the photodissociation of DI are very similar to those arising from HI photodissociation across the energy range spanning the *A* band absorption. On the other hand, the $\mathbf{a}_Q^{(2)}(\perp)$ parameters describing the ground state iodine fragment differ in sign for HI and DI. Similar behavior is seen for the $\mathrm{Im}[\mathbf{a}_1^{(1)}(\parallel,\perp)]$ parameter describing the excited state iodine atom resulting from the dissociation of HI and DI. Despite the fact that the orbital alignment of the iodine fragment will degrade by coupling to the nuclear spin, it should be experimentally feasible to measure the anisotropy parameters. In particular, the sharp differences between HI and DI, i.e., parameters which differ in sign, should be amenable to experimental observation. These experimental measurements would provide direct evidence for or against the current model proposed for the PECs and transition dipole moments of HI. They could also provide further confirmation, or possibly even refutation, of the assumption of adiabatic photodissociation dynamics. We have also presented predictions regarding the production of *both* highly spin polarized H and D atoms from the dissociation of HI and DI. Previously, it has been shown[30,34] that highly spin polarized hydrogen can be produced from the photodissociation of HCl–D atoms produced from the dissociation of DCl

are not spin polarized.[34] All of these results are based on the best available empirical PECs and transition dipole moments for HI.[17] They await experimental verification which will provide a further test of the current model.

Although results have only been presented for excitation from $v=0$, calculations have also been performed for photodissociation of vibrationally excited HI and DI in their $v=1$ states.[61] As has been determined for other properties, e.g., branching fractions and total cross sections, for the vibrationally mediated photodissociation of the hydrogen halides,[18,37,62–65] sharp changes in the properties are observed over narrow photon energy ranges due to nodes in the initial vibrational state. Similar behavior is seen[61] for the $\mathbf{a}_Q^{(K)}(p)$ parameters for HI and DI—see the analogous result for HF and DF given in Ref. 35.

During the review of this paper, a joint experimental and theoretical study[66] of the vibrationally mediated photodissociation of HI appeared in the literature. The experiments measured the branching ratios and anisotropy parameters for the photodissociation of HI ($v=2, J=0$) over the wavelength range 297–350 nm (28 571–33 670 cm^{-1}). In the accompanying theoretical work, it was shown that Leroy's original model[17] could not properly account for these new experimental measurements. Therefore, two new empirical models for the radial dependence of the excited state potential energy curves and transition dipole moments were developed. Both models could account for all of the existing experimental data. Importantly, the wavelength ranges where measurements of the branching ratio would distinguish between the two models were identified for particular initial vibrational states of HI. The wavelength range for which the predictions of the two models differed was shown to increase when photoexcitation occurred from higher initial values of v; explicit results were given for $v=0$–4. The $\mathbf{a}_Q^{(K)}(p)$ parameters are extremely sensitive to the details of the potential energy curves and transition dipole moments and, as shown in Sec. III, are more sensitive than measurement of the total cross section, branching fraction, or the anisotropy parameter β. For example, the $\mathbf{a}_2^{(K)}(\perp)$ parameters are sensitive to the phase difference between the photofragmentation **T** matrix elements for the $a\,^3\Pi_1$ and $A\,^1\Pi_1$ states not just the magnitudes of the corresponding partial cross-sections. Therefore, measurement of the $\mathbf{a}_Q^{(K)}(p)$ parameters, and, in particular, the coherent anisotropy parameters $\mathbf{a}_2^{(K)}(\perp)$ and $\mathbf{a}_1^{(1)}(\parallel, \perp)$, may allow the distinction between the two models over wider wavelength ranges and for lower energies for excitation from $v=0$. However, since the main difference between the two new models and the one utilized here is reflected in measurements corresponding to excitation from initial $v>0$ states,[66] the results presented here for $v=0$, and, in particular, the predicted incoherent anisotropy parameters, should remain valid for energies below $\approx 45\,000\ \mathrm{cm}^{-1}$. Detailed calculations of the $\mathbf{a}_Q^{(K)}(p)$ parameters for $v=0$–4 for both HI and DI using the two new empirical models for the potential energy curves and transition dipole moments are underway.

ACKNOWLEDGMENTS

The author thanks G. G. Balint-Kurti (University of Bristol), O. S. Vasyutinskii (Ioffe Physico-Technical Institute), and T. P. Rakitzis (University of Crete) for useful discussions. The author also thanks the University of Alberta for financial support.

[1] J. Romand, C. R. Acad. Sci. **227**, 117 (1948).
[2] W. C. Price, Proc. R. Soc. London, Ser. A London, Ser. A **167**, 216 (1938).
[3] S. G. Tilford, M. L. Ginter, and A. M. Bass, J. Mol. Spectrosc. **34**, 327 (1970).
[4] J. F. Ogilvie, Trans. Faraday Soc. **67**, 2205 (1971).
[5] S. Manzhos, H. P. Loock, B. L. G. Bakker, and D. H. Parker, J. Chem. Phys. **117**, 9347 (2002).
[6] P. M. Regan, D. Ascenzi, C. Celmenti, M. N. R. Ashfold, and A. J. Orr-Ewing, Chem. Phys. Lett. **315**, 187 (1999).
[7] A. J. R. Heck and D. W. Chandler, Annu. Rev. Phys. Chem. **46**, 335 (1995).
[8] C. A. Wight and S. R. Leone, J. Chem. Phys. **79**, 4823 (1983).
[9] S. R. Langford, P. M. Regan, A. J. Orr-Ewing, and M. N. R. Ashfold, Chem. Phys. **231**, 245 (1998).
[10] D. J. Gendron and J. W. Hepburn, J. Chem. Phys. **109**, 7205 (1998).
[11] R. D. Clear, S. J. Riley, and K. R. Wilson, J. Chem. Phys. **63**, 1340 (1975).
[12] G. N. A. van Veen, K. A. Mohamed, T. Baller, and A. E. deVries, Chem. Phys. **80**, 113 (1983).
[13] T. N. Kitsopoulos, M. A. Buntine, D. P. Baldwin, R. N. Zare, and D. W. Chandler, Proc. SPIE **1858**, 2 (1993).
[14] Z. Xu, B. Koplitz, and C. Wittig, J. Phys. Chem. **92**, 5518 (1988).
[15] R. Schmiedl, H. Dugan, W. Meier, and K. H. Welge, Z. Phys. A **304**, 137 (1982).
[16] R. S. Mulliken, Phys. Rev. **51**, 310 (1937).
[17] R. J. LeRoy, G. T. Kraemer, and S. Manzhos, J. Chem. Phys. **117**, 9353 (2002).
[18] A. B. Alekseyev, H. P. Liebermann, D. B. Kokh, and R. J. Buenker, J. Chem. Phys. **113**, 6174 (2000).
[19] I. Levy and M. Shapiro, J. Chem. Phys. **89**, 2900 (1988).
[20] D. A. Chapman, K. Balasubramanian, and S. H. Lin, Chem. Phys. Lett. **118**, 192 (1985).
[21] D. A. Chapman, K. Balasubramanian, and S. H. Lin, J. Chem. Phys. **87**, 5325 (1987).
[22] D. A. Chapman, K. Balasubramanian, and S. H. Lin, Phys. Rev. A **38**, 6098 (1988).
[23] T. P. Rakitzis, S. A. Kandel, A. J. Alexander, Z. H. Kim, and R. N. Zare, J. Chem. Phys. **110**, 3351 (1999).
[24] T. P. Rakitzis and T. N. Kitsopoulos, J. Chem. Phys. **116**, 9228 (2002).
[25] A. S. Bracker, E. R. Wouters, A. G. Suits, and O. S. Vasyutinskii, J. Chem. Phys. **110**, 6749 (1999).
[26] M. J. Bass, M. Brouard, A. P. Clark, C. Vallance, and B. Martinez-Haya, Phys. Chem. Chem. Phys. **5**, 856 (2003).
[27] A. S. Bracker, E. R. Wouters, A. G. Suits, Y. T. Lee, and O. S. Vasyutinskii, Phys. Rev. Lett. **80**, 1626 (1998).
[28] A. J. Alexander, Z. H. Kim, S. A. Kandel, R. N. Zare, Y. Asano, and S. Yabushita, J. Chem. Phys. **113**, 9022 (2000).
[29] T. P. Rakitzis, P. C. Samrtzis, R. L. Toomes *et al.*, Chem. Phys. Lett. **364**, 115 (2002).
[30] T. P. Rakitzis, P. C. Samartzis, R. L. Toomes, T. N. Kitsopoulos, A. Brown, G. G. Balint-Kurti, O. S. Vasyutinskii, and J. A. Beswick, Science **300**, 1936 (2003).
[31] L. D. A. Siebbeles, M. Glass-Maujean, O. S. Vasyutinskii, J. A. Beswick, and O. Roncero, J. Chem. Phys. **100**, 3610 (1994).
[32] T. P. Rakitzis and R. N. Zare, J. Chem. Phys. **110**, 3341 (1999).
[33] E. R. Wouters, M. Ahmed, D. S. Peterska, A. S. Bracker, A. G. Suits, and O. S. Vasyutinskii, in *Imaging in Chemical Dynamics*, edited by A. G. Suits and R. E. Continetti (American Chemical Society, Washington, DC, 2000), p. 238.
[34] A. Brown, G. G. Balint-Kurti, and O. S. Vasyutiniskii, J. Phys. Chem. A **108**, 7790 (2004).
[35] G. G. Balint-Kurti, A. J. Orr-Ewing, J. A. Beswick, A. Brown, and O. S. Vasyutinskii, J. Chem. Phys. **116**, 10760 (2002).
[36] A. Brown and G. G. Balint-Kurti, J. Chem. Phys. **113**, 1870 (2001).
[37] P. M. Regan, D. Ascenzi, A. Brown, G. G. Balint-Kurti, and A. J. Orr-Ewing, J. Chem. Phys. **112**, 10259 (2000).
[38] C. E. Moore, *Atomic Energy Levels* (U.S. GPO, Washington, DC, 1971).
[39] C. F. Goodeve and A. W. C. Taylor, Proc. R. Soc. London, Ser. A London, Ser. A **154**, 181 (1936).

[40]J. Romand, Ann. Phys. (Paris) **4**, 527 (1948).
[41]D. V. Kupriayanov, B. N. Sevastianov, and O. S. Vasyutinskii, Z. Phys. D: At., Mol. Clusters **15**, 105 (1990).
[42]G. G. Balint-Kurti, R. N. Dixon, and C. C. Marston, Int. Rev. Phys. Chem. **11**, 317 (1992).
[43]G. G. Balint-Kurti, R. N. Dixon, and C. C. Marston, J. Chem. Soc., Faraday Trans. **86**, 1741 (1990).
[44]E. J. Heller, J. Chem. Phys. **68**, 2066 (1978).
[45]E. J. Heller, J. Chem. Phys. **68**, 3891 (1978).
[46]E. J. Heller, Acc. Chem. Res. **14**, 368 (1981).
[47]G. G. Balint-Kurti, Adv. Chem. Phys. **128**, 249 (2003).
[48]A. Brown and G. G. Balint-Kurti, J. Chem. Phys. **113**, 1879 (2001).
[49]C. C. Marston and G. G. Balint-Kurti, J. Chem. Phys. **91**, 3571 (1989).
[50]G. G. Balint-Kurti, C. L. Ward, and C. C. Marston, Comput. Phys. Commun. **67**, 285 (1991).
[51]H. Tal-Ezer and R. Kosloff, J. Chem. Phys. **81**, 3967 (1984).
[52]R. Kosloff, J. Phys. Chem. **92**, 2087 (1988).
[53]Temperature dependent data at 10, 300, and 1000 K taken from EPAPS Document No. E-JCPSA6-117-002243.
[54]B. V. Picheyev, A. G. Smolin, and O. S. Vasyutinskii, J. Phys. Chem. A **101**, 7614 (1997).
[55]K. Blum, *Density Matrix Theory and Applications*, 2nd ed. (Plenum, New York, 1990).
[56]R. N. Zare, *Angular Momentum* (World Scientific, New York, 1988).
[57]A. R. Edmonds, *Angular Momentum in Quantum Mechanics* (Princeton University Press, Princeton, 1960).
[58]H. Rottke and H. Zacharias, Phys. Rev. A **33**, 736 (1986).
[59]W. Happer, Rev. Mod. Phys. **44**, 169 (1972).
[60]See EPAPS Document No. E-JCPSA6-122-010507 for the numerical data contained in Figs. 6–9, i. e., the anisotropy parameters for $I(^2P_{3/2})$, $I(^2P_{1/2})$ and H/D produced from the photodissociation of HI and DI as a function of photolysis energy. A direct link to this document may be found in the online article's HTML reference section. The document may also be reached via the EPAPS homepage (http://www.aip.org/pubservs/epaps.html) or from ftp.aip.org in the directory/epaps. See the EPAPS homepage for more information.
[61]A. Brown (unpublished).
[62]S. C. Givertz and G. G. Balint-Kurti, J. Chem. Soc., Faraday Trans. 2 **82**, 1231 (1986).
[63]I. H. Gersonde, S. Henning, and H. Gabriel, J. Chem. Phys. **101**, 9558 (1994).
[64]B. Pouilly and M. Monnerville, Chem. Phys. **238**, 437 (1998).
[65]C. Kalyanaraman and N. Sathyamurthy, Chem. Phys. Lett. **209**, 52 (1993).
[66]J. P. Camden, H. A. Bechtel, D. J. A. Brown, A. E. Pomerantz, R. N. Zare, and R. J. LeRoy, J. Phys. Chem. A **108**, 7806 (2004).